J Mol Model (2014) 20:2543
DOI 10.1007/s00894-014-2543-7

ORIGINAL PAPER

A DFT study on surface dependence of β-Ga_2O_3 for CO_2 hydrogenation to CH_3OH

Jin Qu · Shik Chi Edman Tsang · Xue-Qing Gong

Received: 28 September 2014 / Accepted: 24 November 2014 / Published online: 6 December 2014

Abstract In this paper, the catalytic activities of various β-Ga_2O_3 surfaces for CO_2 hydrogenation have been studied by density functional theory (DFT) calculations. The surface dependence of adsorptions and coadsorptions of reactants are investigated on two terminations of Ga_2O_3, which are Ga_2O_3(001) and Ga_2O_3(111). The active termination of Ga_2O_3(001) is identified and a surface structure rearrangement is determined. The thermodynamic profiles of surface intermediates involved in the reaction pathways for methanol formation are systematically calculated, and the initial key step of CO_2 hydrogenation to bicarbonate is analyzed in detail. It has been found that the active Ga_2O_3(001) termination gives rise to a lower hydrogenation barrier largely due to the fact that saturated lattice O at Ga_2O_3(001) can act as a favorable site for both hydrogen adsorption and transfer while the unsaturated O at Ga_2O_3(111) is much less effective for these processes.

Keywords CO_2 activation · Density functional theory · β-Gallium oxide · Methanol formation

Electronic supplementary material The online version of this article (doi:10.1007/s00894-014-2543-7) contains supplementary material, which is available to authorized users.

J. Qu · X.-Q. Gong (✉)
Key Laboratory for Advanced Materials, Centre for Computational Chemistry and Research Institute of Industrial Catalysis, East China University of Science and Technology, 130 Meilong Road, Shanghai 200237, People's Republic of China
e-mail: xgong@ecust.edu.cn

J. Qu · S. C. E. Tsang
Department of Chemistry, University of Oxford, Oxford OX1 3QR, UK

Introduction

Gallium oxide (Ga_2O_3) is an important wide band gap (4.2-4.9 eV) semiconductor [1–3]. Among its different polymorphs, only the monoclinic β phase is stable at high temperatures up to its melting point, and it has drawn a lot of attention for its potential application as optoelectronic devices [4, 5], gas sensors [6, 7], spintronic devices [8, 9], etc. Besides experimental studies, many theoretical simulations using first principles calculations have been carried out to explore its structural [10, 11], electronic [12], and optical [13] properties.

In recent decades, Ga_2O_3 has also been particularly noted for its catalytic activity in CO_2 hydrogenation [14]. It is even expected to be able to compete with the classical industrial Cu/ZnO catalysts [15]. Several reaction pathways have been proposed to explain its catalytic mechanism [16–19]. Infrared (IR) spectroscopy studies of Ga_2O_3 based catalysts have identified different surface reaction intermediate species such as formate, carbonate, and bicarbonate in various adsorption states [20]. Moreover, when Ga_2O_3 supported Pd nanoparticles were used, active hydrogen species spilled over from supported metal were found to accelerate the reaction [20, 21], and the formation of surface Pd-Ga alloy at high temperatures was also proposed to explain the high activity [22]. The occurrence of carbonate and bicarbonate species was believed to be the indication of CO_2 activation [23]. Accordingly, the addition of other oxides which could enhance the adsorption of CO_2 and the formation of these intermediates over Ga_2O_3 was studied [24]. The hydrogenation of formate to methylenebisoxy was also identified as a possible rate determining step when the amount of active H was sufficient [25]. It has also been proposed that surface oxygen vacancies which could enhance CO_2 adsorption and H_2 dissociation might play a crucial role in this reaction as well [26–29].

Adsorbate behaviors on Ga_2O_3 such as CO_2 [27], CH_4 [30], H_2 [28, 29, 31], formate [32], CH_3OH [33] etc. have been investigated by using different theoretical methods. Most of these simulations were based on the lowest-energy (100) termination surface of β-Ga_2O_3 [11]. With combined experimental and computational methods, H_2O, alcohols, and carboxylic acids on different terminations of Ga_2O_3(100) have also been studied [34]. It has been found that the adsorption strength is very sensitive to the surface termination and the less stable surface is more reactive. More recently, thin films with different Ga_2O_3 surface orientations such as (100), ($\bar{2}$ 01) and (001) were successfully prepared [35, 36], and various shapes of Ga_2O_3 nanostructures have also been constructed [37–45]. A plate like Ga_2O_3 material with dominating {001} facets has been reported to be much more active and exhibit stronger metal-support interaction compared to the {111} dominated nanorod [46]. It is therefore crucial to understand the promoting effect of Ga_2O_3(001) facet as it might lead us to some new understanding of this material in catalysis.

In this work, we performed systematic density functional theory (DFT) calculations of the adsorption of reactants and intermediates involved in the hydrogenation of CO_2 at β-Ga_2O_3(001). We also attempted to compare the key steps of CO_2 activation on different β-Ga_2O_3(001) and (111) surfaces, which may shed light on the origin of the catalytic properties of low index β-Ga_2O_3 surfaces and their roles in the plate and nanorod like materials.

Computational details

All calculations were conducted in the framework of DFT by using the Vienna ab initio simulation package (VASP) [47–50]. The projector-augmented wave (PAW) potentials [51, 52] were used for the core electron interaction. The Perdew–Burke–Ernzerhof (PBE) functional [53, 54] based on the generalized gradient approximation (GGA) was employed to evaluate the non-local exchange-correlation energy. For all structural optimizations, a plane wave basis set with a cutoff energy of 400 eV was used and the ionic positions were allowed to relax until the forces were less than 0.02 eV/Å. Spin polarization was also included in all calculations, and Bader charge analyses [55–58] were applied to study the charge distribution. The nudged elastic band (NEB) method was used to determine the transition states (TS) along the reaction pathways [59–64].

In this work, the unit cell model for the bulk monoclinic β-Ga_2O_3 contained four Ga_2O_3 units (see Fig. 1). A 2×8×4 k-point grid determined by the Monkhorst-Pack method was used in the bulk cell optimization, which gave rise to cell parameters of a=12.255 Å, b=3.052 Å, c=5.828 Å, in good agreement with the experimental values (a=12.230 Å, b=3.040 Å, c=5.800 Å). There are two inequivalent Ga sites (tetrahedral Ga(I) and octahedral Ga(II)) and three inequivalent O sites (out of plane of Ga triangle O(I), in the plane of Ga triangle O(II) and tetrahedral O(III)) in each unit cell as shown in Fig. 1.

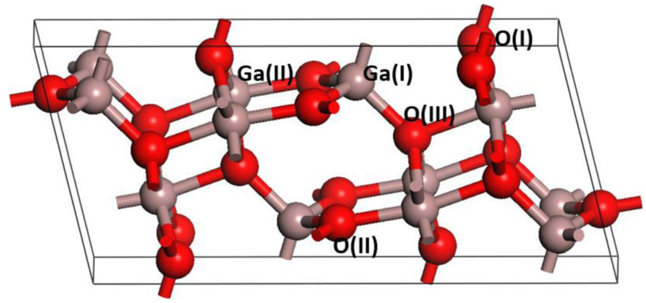

Fig. 1 Bulk unit cell of monoclinic β-Ga_2O_3. The pink balls denote Ga atoms and the red balls are O. Different Ga and O atoms are labeled

Two different Ga_2O_3(001) terminations were built as described in ref. [11], namely (001)-A and (001)-B. The 2×2 surface supercell (12.630×6.104 Å^2) was used in this study for both (001) slabs. To study the Ga_2O_3(111) surface, we built a stoichiometric unreconstructed Ga_2O_3(111) slab containing three eight-member rings and one four-member ring on the termination in each surface cell. A 2×1 supercell (12.630×6.578 Å^2) was used to make the surface size similar to that of Ga_2O_3(001). The bulk-truncated models of these three surfaces could be found in Supporting information (SI) (see Fig. S1) and distinct surface Ga and O sites are labeled. The changes of the coordination number of surface atoms with respect to the corresponding bulk atoms are summarized in Table 1.

Both Ga_2O_3(001) and (111) surfaces were modeled by periodic slab models with 24 Ga_2O_3 molecular units being distributed in six Ga layers. The bottom two layers were frozen at their bulk positions while the top four layers were allowed to relax in all calculations. The *k*-point sampling used a 2×4×1 grid, and a vacuum layer of 12 Å along the z direction perpendicular to the surface was employed to prevent spurious interactions between the repeated slabs in all these models.

To estimate the adsorption energies, the following equation was considered:

Table 1 Coordination number changes of Ga_2O_3 surface atoms (bulk-surface)

O number	(001)-A	(001)-B	(111)	Ga number	(001)-A	(001)-B	(111)
1	3 – 2	4 – 2	3 – 2	1	4 – 3	6 – 4	4 – 3
2	3 – 3	3 – 3	3 – 2	2	6 – 6	4 – 4	6 – 5
3	4 – 4	3 – 3	4 – 3	3			6 – 5
4			4 – 4	4			4 – 4
5			3 – 3				
6			3 – 3				

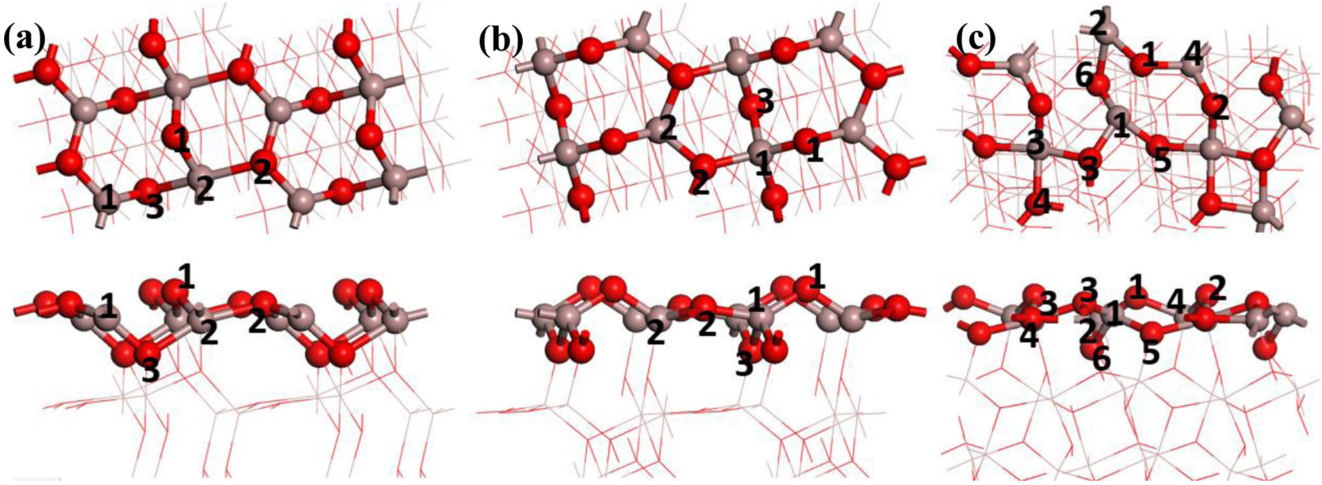

Fig. 2 Top and side views of surface structures of bulk-truncated Ga_2O_3 (**a**) (001)-A, (**b**) (001)-B, and (**c**) (111) after optimization

$$E_{ads} = -(E_{slab+mol} - (E_{slab} + E_{mol})),$$

in which E_{slab} and E_{mol} are the total energies of Ga_2O_3 surface slab and a single adsorbate molecule in gas phase; $E_{slab+mol}$ denotes the total energy of slab with adsorbed molecule.

Results and discussion

Bare (001)-A, (001)-B, and (111) surfaces of Ga_2O_3

The optimized structures of bare Ga_2O_3(001) surface with two different bulk-truncated terminations, namely Ga_2O_3(001)-A and (001)-B, are presented in Fig. 2. For Ga_2O_3(001)-A (Fig. 2(a)), the most distorted part after optimization is around the Ga1 site. The O2 atom shifts up by 0.635 Å while the Ga1 atom bends down by 0.075 Å, contracting and averaging the three Ga-O bond lengths (1.812 Å, 1.812 Å, 1.801 Å) of Ga1 from 1.839 Å, 1.839 Å, and 1.860 Å, respectively, and creating a planer triangle like coordination environment. This is mainly due to the fact that Ga1 is type I tetrahedral Ga in the bulk which bears coordination decrease on the surface while Ga2 keeps all its surrounding octahedral oxygen.

It needs to be noted that this Ga_2O_3(001)-A surface can undergo a further asymmetric distortion (see Fig. 3) when the CO_2 molecule adsorbs on it (Fig. 4(a)). We then optimized the adsorption-induced reconstructed surface and found that the rearrangements of surface atoms can further reduce the total energy of the clean surface slab by around 2 eV. As presented in Fig. 3, the Ga2' atom shifts by 1.096 Å along the [010] direction, which elongates the bond between Ga2' and O3' from 2.099 to 3.013 Å. The corresponding Ga2-O3 bond beside the adsorbate area is decreased to 2.001 Å, which also reduces the Ga1-O1 distance to 1.912 Å to form a tetrahedral like coordination for Ga1. Moreover, the O3 and O3' atoms further drop below the surface, which may make them more difficult to be reached by other reactants. It needs to be mentioned that such reconstruction could also be identified when other reaction intermediates such as HCOO, COOH, and HCO (see below) adsorb at Ga_2O_3(001)-A. Thus we used the optimized rearranged surface as reference when we calculated adsorption energies on this surface.

The Ga_2O_3(001)-B (Fig. 2(b)) termination exhibits slight fluctuation after optimization, especially at its Ga1 site. The Ga1 atom here is a type II octahedral Ga in the bulk and it has two lattice oxygen removed on the surface. It embeds into the surface by 0.214 Å and the angles of O1-Ga1-O3, O2-Ga1-O3, and O3-Ga1-O3 change from 91.0°, 95.5°, and 100.4° in the bulk to 104.8°, 97.8°, and 109.4°, respectively, indicating a trend for the Ga1 to evolve to tetrahedral coordination for stabilization.

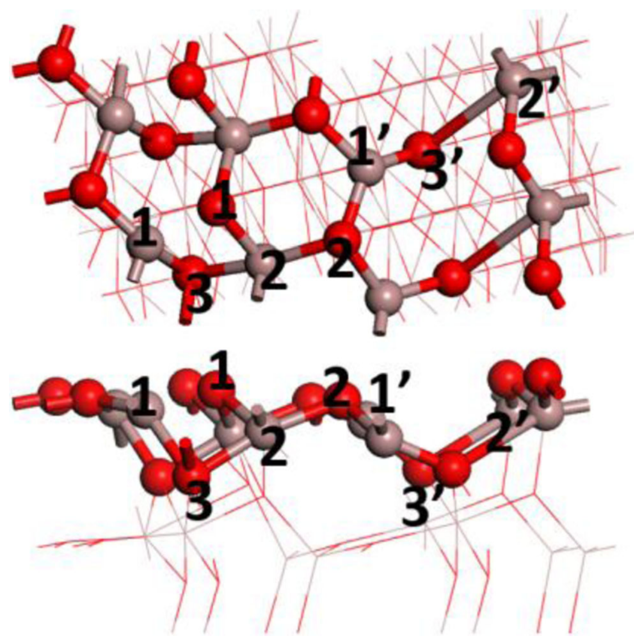

Fig. 3 Top and side views of calculated rearranged surface structure of Ga_2O_3 (001)-A

Table 2 Calculated Bader charges (in |e|) of surface and bulk Ga

Ga number	(001)-A		(001)-B		(111)	
	surface	bulk	surface	bulk	surface	Bulk
1	1.77	1.82	1.82	1.89	1.77	1.83
2	1.81	1.90	1.80	1.82	1.82	1.88
3					1.84	1.90
4					1.79	1.83

The Ga_2O_3(111) structure bears a more complicated coordination change for the surface atoms compared with those in the bulk. All four exposed Ga rise up along the surface normal vector (Fig. 2(c)). The movement of these Ga pushes O1 atom to the center of Ga1-Ga2-Ga4 triangle and reduces the Ga1-O1 distance from 3.515 Å to 2.192 Å, which produces a bond compensation for the tetrahedral Ga1 while maintaining the coordination environment of Ga2 and Ga4.

The Bader charge analyses (Table 2) unsurprisingly showed that for all three slabs the Ga atoms on the surfaces are less positive than their counterparts in the bulk, indicating slight reduction of surfaces. Moreover, the charge of sixfold coordinated Ga2 on Ga_2O_3(001)-A changed the most significantly which may be due to the stretching of its surrounding bonds.

Adsorptions and surface reactions

Adsorptions of hydrogen and CO_2 on Ga_2O_3(001)-A, (001)-B, and (111) surfaces

According to our calculations, H_2 molecule adsorbs rather weakly on these Ga_2O_3 surfaces. The calculated H_2 adsorption energies at Ga_2O_3(001)-A, (001)-B, and (111) are 0.04 eV, 0.05 eV, and 0.04 eV, respectively, and the distances between H_2 and surface O atoms are all longer than 2.4 Å (calculated structures are presented in Fig. S2). For H atom, the most stable adsorption sites are always the unsaturated O1 of the surfaces and the adsorption processes are all exothermic. The corresponding adsorption energies (with respect to half H_2) are 0.75 eV at Ga_2O_3(001)-A, 0.26 eV at (001)-B, and 0.63 eV at (111) surface. The Ga_2O_3(001)-A gives the highest adsorption energy which could favor hydrogen spillover from supported metal. We also tested various Ga sites for H atom adsorption. However, all those processes are endothermic or the H atom moves to O sites beside the Ga after optimization.

For CO_2 adsorption, our calculation showed that Ga_2O_3(111) gives the strongest adsorption. The adsorption energy is 0.94 eV on it, while it is 0.92 eV on Ga_2O_3(001)-A and only 0.17 eV on Ga_2O_3(001)-B. In Fig. 4, we present the calculated structures of CO_2 adsorption at these surfaces. The blue balls denote the O atoms in CO_2. As one may expect from the adsorption structures, the bending of the CO_2 forms a carbonate-like species accompanied by electron transfer to the molecule, which may give rise to its strong interaction with the surface. The bended CO_2 on both Ga_2O_3(001)-A and Ga_2O_3(111) sits at the least positive Ga atom of each surface. The Bader charge analyses showed that all the adsorbed CO_2 are negative, and calculated charges are −0.19 |e| and −0.20 |e| at Ga_2O_3(001)-A and (111), respectively. While for the weakly adsorbed linear CO_2 on Ga_2O_3(001)-B, the calculated charge is only −0.01 |e|, which suggests the nature of a neutral molecule. The charges transferred from the surfaces could therefore activate the CO_2 and lead to further reactions.

Coadsorption of H atom and CO_2 molecule on Ga_2O_3(001)-A, (001)-B, and (111) surfaces

Based on the most stable adsorption structures of CO_2 on the three Ga_2O_3 surfaces, we tried various coadsorption configurations of H atom and CO_2 molecule. Since the adsorption of H_2 is generally very weak, H atoms involved in the

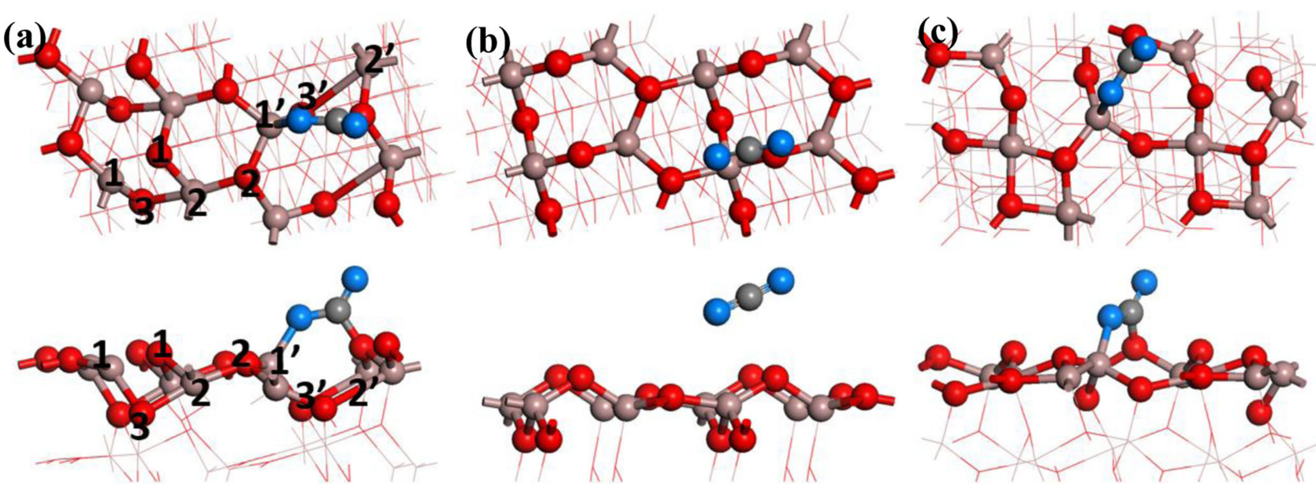

Fig. 4 Top and side views of the most stable CO_2 adsorption structures on Ga_2O_3 (**a**) (001)-A, (**b**) (001)-B, and (**c**) (111). O of CO_2 are in blue

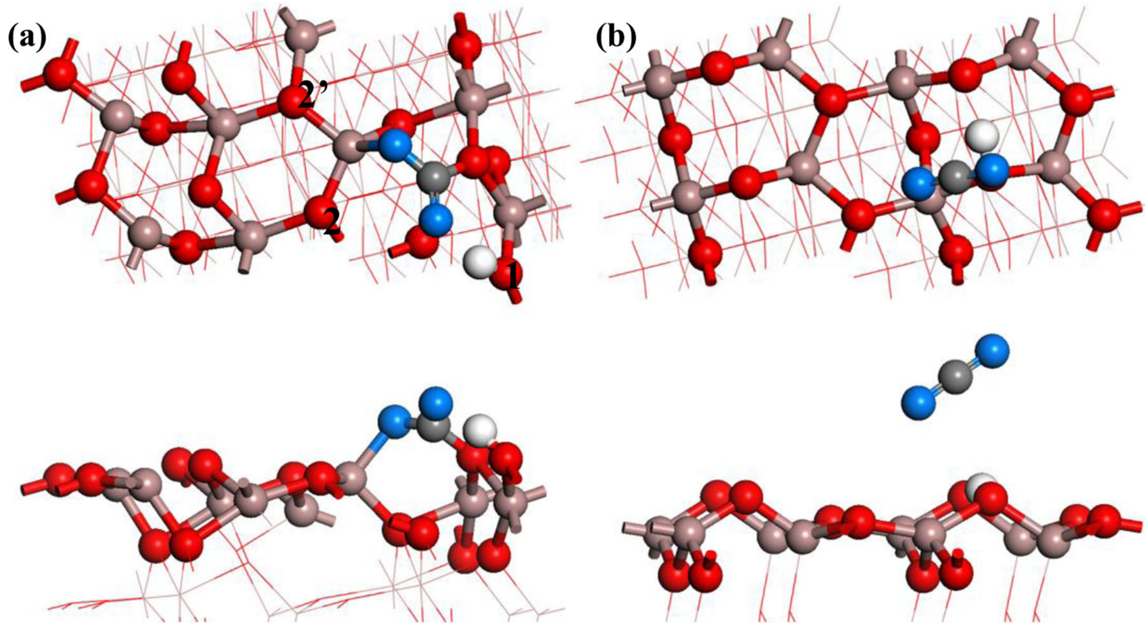

Fig. 5 Top and side views of the most stable CO_2+H coadsorption structures at Ga_2O_3 (**a**) (001)-A and (**b**) (001)-B

hydrogenation processes are very likely to spill from supported metal clusters [20]. These coadsorption structures could then be the initial states of further hydrogenation reactions. The most favorable coadsorption structures at Ga_2O_3(001)-A and (001)-B are presented in Fig. 5. At Ga_2O_3(001)-A, the coadsorption energy is 1.74 eV and the distance between the adsorbed H and the nearest O atom of neighboring CO_2 is 1.783 Å. This carbonate-like adsorbed CO_2 molecule tilts down to the H and the coadsorption forms a very stable structure on the surface. It is energetically 0.67 eV more stable than the COOH intermediate (SI, Fig. S3(b)), and the barrier for the H to transfer to form such COOH is as high as ~2.5 eV. Thus the H atom could hardly move to CO_2 to undergo further reactions and this strongly adsorbed co-adsorption intermediate tends to be eventually stuck in this structure. However, there are actually five O sites around the adsorbed CO_2 (Fig. 5(a)), among which the O2 and O2' (type II) and the O1 (type I) may also be the sites for H adsorption and the distances between such H and O in CO_2 are within 3 Å. We then expected another co-adsorption structure presented in

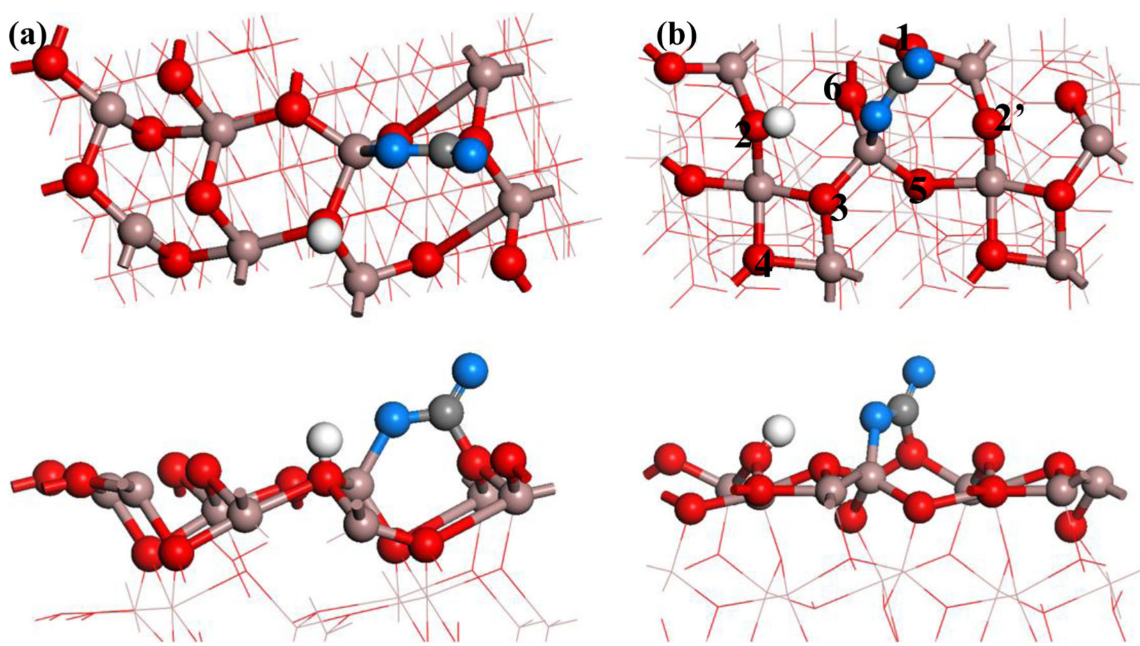

Fig. 6 Top and side views of coadsorption structures as initial states for the following reactions at Ga_2O_3 (**a**) (001)-A and (**b**) (111)

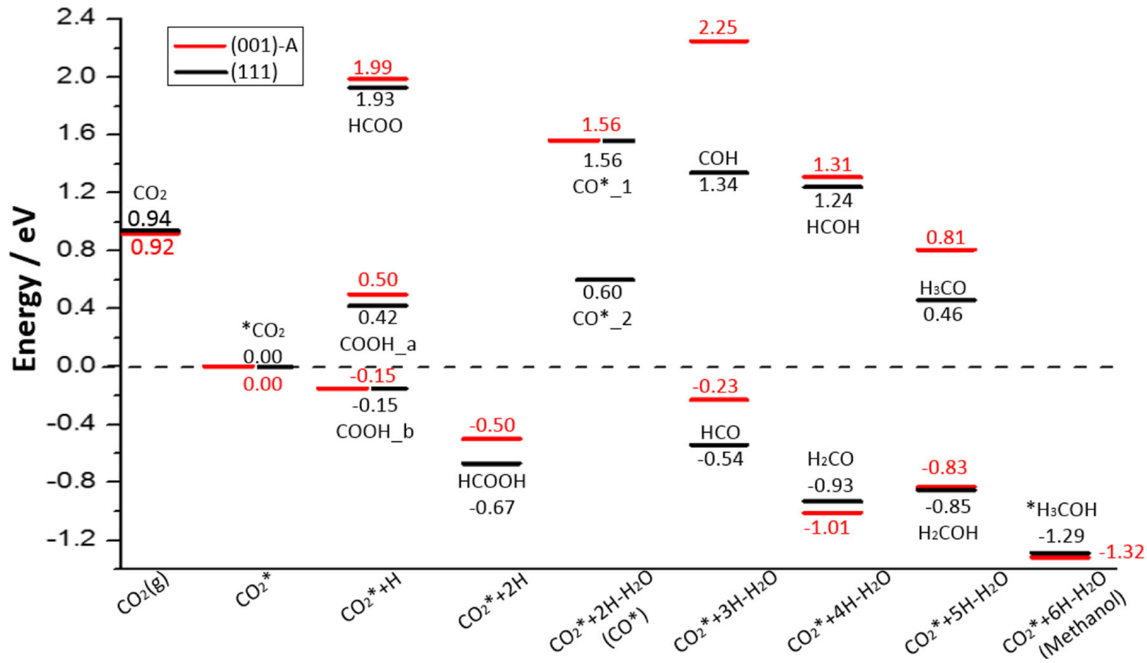

Fig. 7 Calculated relative energies of the intermediates adsorbed at Ga_2O_3 (001)-A and (111)

Fig. 6(a) to be the initial state for the hydrogenation reaction at Ga_2O_3(001)-A. In this second most stable co-adsorption configuration at Ga_2O_3(001)-A, the H sits on the saturated O2 next to the CO_2. The corresponding co-adsorption energy was calculated to be 0.50 eV and the distance between H and the nearest O of CO_2 is 2.750 Å. On the other hand, the CO_2 coadsorbs with H atom weakly on Ga_2O_3(001)-B (Fig. 5(b)). The adsorption energy is 0.56 eV, and the distance between H and the lower O in CO_2 is 3.042 Å while the H-C distance is 3.177 Å. Also, the CO_2 molecule still keeps a linear configuration and the H atom is actually embed in between two O atoms, which makes it even harder to approach the CO_2. Then, from the calculated co-adsorption structures of H and CO_2, one can expect that the Ga_2O_3(001)-A could play a more crucial role than (001)-B in CO_2 hydrogenation to CH_3OH.

It needs to be noted that at Ga_2O_3(111), the most favorable H adsorption site O1 is blocked by pre-adsorbed CO_2. Among the O sites around the adsorbed CO_2, only two of them can hold the H with the distance between H and O in CO_2 less than 3 Å, which are O2 (type I) and O3 (type III). The most favorable coadsorbed H atom sits on surface O2 (Fig. 6(b)), which gives independent H adsorption energy of 0.49 eV. Correspondingly, the calculated coadsoprtion energy is 1.42 eV, which does not show any promotion effect with respect to the separate adsorptions, and the distance between H and the nearest O of CO_2 is 2.703 Å. This coadsorption is quite similar to that at Ga_2O_3(001)-A (Fig. 6(a)) and we took it as the initial state for the CO_2 hydrogenation at Ga_2O_3(111).

Hydrogenation of CO_2 on Ga_2O_3(001)-A and (111) surfaces

As the active {001} facet and the initial states are confirmed, we then compared the reactions at Ga_2O_3(001)-A and Ga_2O_3(111). To investigate this process, we added hydrogen

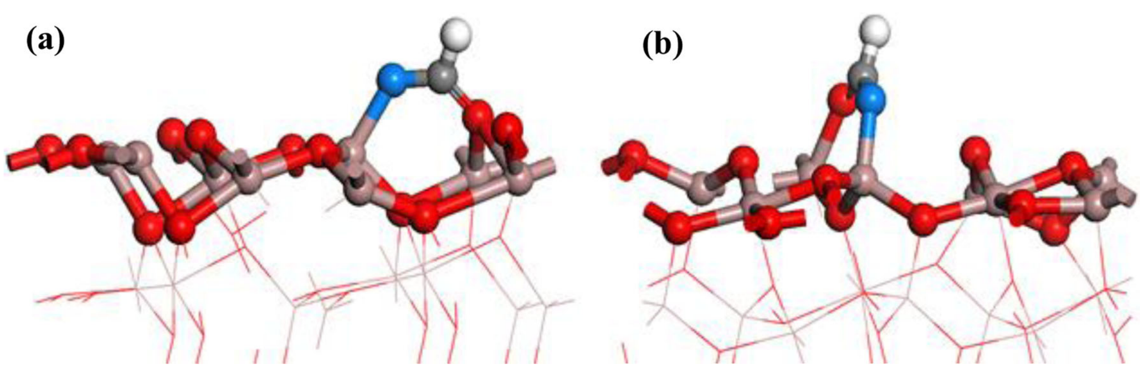

Fig. 8 Calculated strucutres of HCO intermediate at Ga_2O_3 (**a**) (001)-A; (**b**) (111)

atoms to the adsorbed CO_2 one by one and remove water molecule if needed to construct a series of reaction intermediates leading to methanol. The diagram of calculated relative energies is plotted in Fig. 7 and the intermediates structures can be found in SI (Fig. S3-S11). All the energy values listed in Fig. 7 are estimated relative to adsorbed CO_2 on each surface and gas-phase H_2 and H_2O molecules.

One can see from the diagram that the product methanol (Fig. S11) and most of the intermediates in each step have similar relative energies with differences below 0.20 eV. From the thermodynamic point of view, we could identify the lowest-energy reaction route below the zero energy base line along COOH_b (Fig. S3(b), (e)), HCOOH (Fig. S4), HCO (Fig. 8), H_2CO (Fig. S8), H_2COH (Fig. S10), and finally the methanol on these two surfaces. In particular, calculated energies of HCOO intermediates on the two surfaces (Figs. S3(c) and (f)) are approximately 2 eV higher than COOH on the corresponding surfaces, indicating that the latter should be

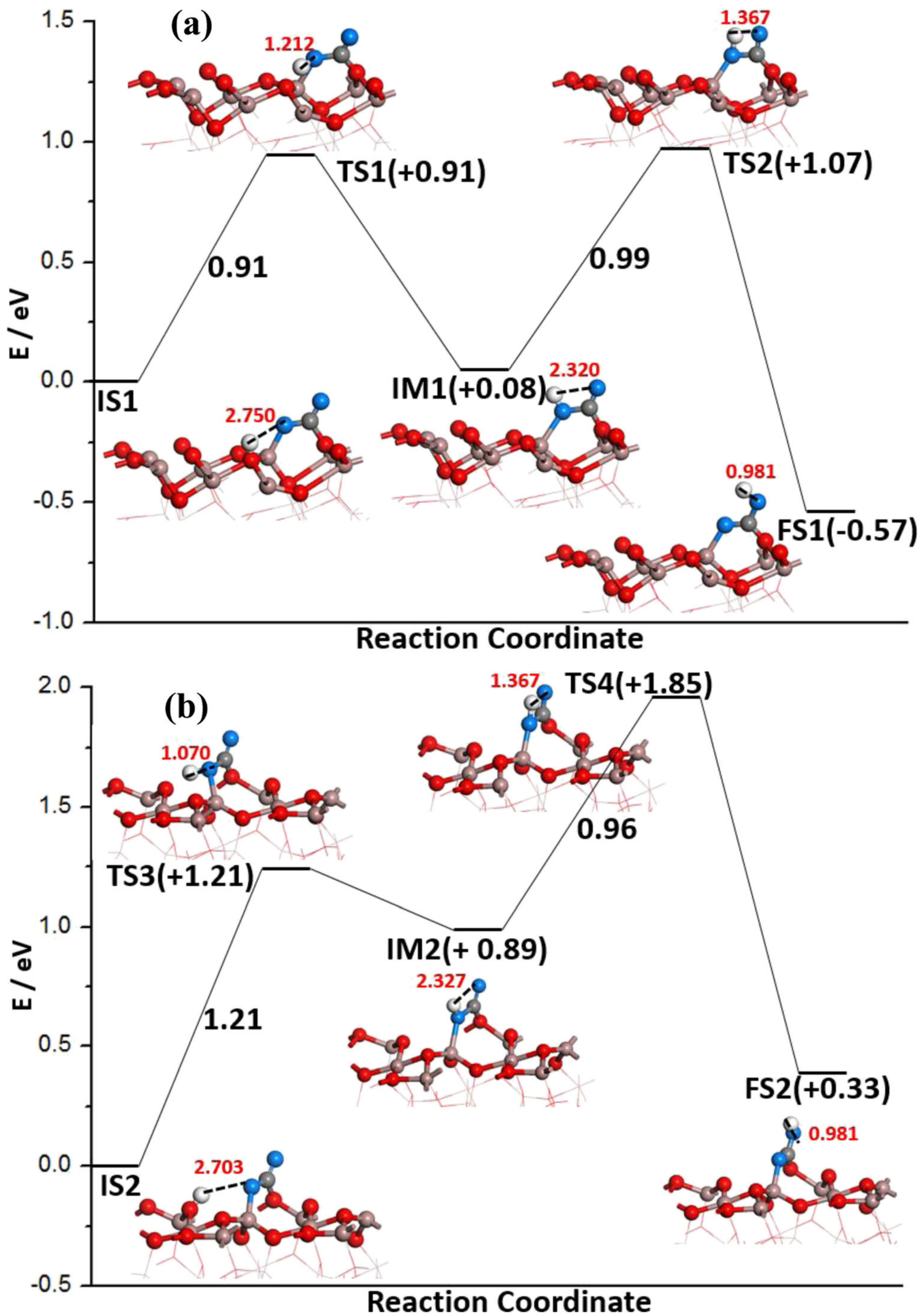

Fig. 9 Calculated potential energy profiles of H transfer at Ga_2O_3 (**a**) (001)-A and (**b**) (111)

more likely to form in the first step of hydrogenation. The activation of CO_2 to such bicarbonate species is therefore a key step during the whole process for methanol formation. It should also be mentioned that the HCO species (Fig. 8) formed as the result of bicarbonate reduction actually gives a formate structure, which could be further hydrogenated to methanol as reported by Collins et al. [20, 22].

The detailed process of H transfer for COOH formation was then calculated. From the initial co-adsorption state (IS), the H could first move to the nearby O of the CO_2 (intermediate, IM) and then diffuse to the upper O, which gives the most favorable final state (FS) as a bicarbonate-like species. These processes are presented in Fig. 9. The related H-O distances are also presented in red.

From the calculated energy profile we can find that the first step of hydrogen transfer is endothermic on both these surfaces. The intermediate state on Ga_2O_3(001)-A is 0.08 eV higher than the initial state after climbing over a barrier of 0.91 eV. By contrast, at Ga_2O_3(111), the intermediate state is 0.89 eV less stable than the initial one and the barrier is 1.21 eV, both of which are higher than the corresponding ones at (001)-A. The diffusion of H within the CO_2 molecule is the second step, which needs to overcome a barrier of 0.99 eV at (001)-A and 0.96 eV at (111). One can see that this inner-molecular H diffusion process is quite similar at the two surfaces as it is obviously very weakly affected by oxide surfaces. The occurrence of the final state is exothermic with respect to the initial state on (001)-A, but it is still endothermic for (111).

The above calculations regarding the first H transfer processes showed that CO_2 hydrogenation is much more favorable to occur at Ga_2O_3(001)-A compared to Ga_2O_3(111). As we have mentioned, among the O sites surrounding the adsorbed CO_2, saturated O2 and O2’ of type II and unsaturated O1 of type I at Ga_2O_3(001)-A could act as the H adsorption sites and give the distances between H and O in CO_2 below 3 Å. Similarly, unsaturated O2 of type I and unsaturated O3 of type III are where the H can co-adsorb at Ga_2O_3(111) with adsorbed CO_2. The advantages of Ga_2O_3(001)-A is mainly due to the fact that the saturated O2 (type II) in a distorted planer triangle coordination environment is energetically more suitable than the two unsaturated O at Ga_2O_3(111) which hold the H too strongly in promoting the hydrogenation transfer. It might also benefit the subsequent steps and finally lead to the higher conversion rate of CO_2 on (001)-A dominated plate like Ga_2O_3.

Conclusions

We have performed systematic DFT calculations to compare β-Ga_2O_3(001) and (111) surfaces in promoting CO_2 hydrogenation to methanol in this work. Our results identified the β-Ga_2O_3(001)-A termination as the active one for Ga_2O_3(001) and showed a face dependence of the catalytic performance of Ga_2O_3 based materials. In particular, the similar bending adsorption structures of CO_2 at Ga_2O_3(001)-A and (111) indicate a charge transfer from surface to molecule and its activation at these two surfaces, while Ga_2O_3(001)-B is much less active for CO_2 adsorption and activation. Moreover, the saturated surface O in a distorted planer triangle coordination environment at Ga_2O_3(001)-A can benefit hydrogen transfer to CO_2, which is the first and key step in the whole process for methanol formation.

Acknowledgments This work was supported by the National Basic Research Program (2011CB808505), National Natural Science Foundation of China (21322307, 21421004), Open Project of State Key Laboratory of Chemical Engineering (SKL-ChE-12C02), and “Shu Guang” project of Shanghai Municipal Education Commission and Shanghai Education Development Foundation (13SG30). The authors are thankful for the computing time in the National Super Computing Center in Jinan. J.Q. also thanks China Scholarship Committee (CSC) for the visiting studentship at Oxford University.

References

1. Tippins HH (1965) Phys Rev 140:A316–A319
2. Kim HG, Kim WT (1987) J Appl Phys 62:2000–2002
3. Ueda N, Hosono H, Waseda R, Kawazoe H (1997) Appl Phys Lett 71:933–935
4. Yusa H, Tsuchiya T, Sata N, Ohishi Y (2008) Phys Rev B 77:064107
5. Kokubun Y, Miura K, Endo F, Nakagomi S (2007) Appl Phys Lett 90:031912
6. Basharat S, Carmalt CJ, Binions R, Palgrave R, Parkin IP (2008) Dalton Trans 5:591–595
7. Mazeina L, Perkins FK, Bermudez VM, Arnold SP, Prokes SM (2010) Langmuir 26:13722–13726
8. Remeika JP (1960) J Appl Phys 31:S263–S264
9. Hayashi H, Huang R, Ikeno H, Oba F, Yoshioka S, Tanaka I, Sonoda S (2006) Appl Phys Lett 89:181903
10. Yoshioka S, Hayashi H, Kuwabara A, Oba F, Matsunaga K, Tanaka I (2007) J Phys Condens Matter 19:346211
11. Bermudez VM (2006) Chem Phys 323:193–203
12. Yamaguchi K (2004) Solid State Commun 131:739–744
13. Rahane AB, Deshpande MD, Chakraborty S (2012) J Phys Chem A 116:10559–10565
14. Fujitani T, Nakamura I (2002) Bull Chem Soc Jpn 75:1393–1398
15. Fujitani T, Saito M, Kanai Y, Watanabe T, Nakamura J, Uchijima T (1995) Appl Catal A Gen 125:L199–L202
16. Yang Y, Evans J, Rodriguez JA, White MG, Liu P (2010) PCCP 12: 9909–9917
17. Grabow LC, Mavrikakis M (2011) ACS Catal 1:365–384
18. Zhao Y-F, Yang Y, Mims C, Peden CHF, Li J, Mei D (2011) J Catal 281:199–211
19. Weigel J, Koeppel RA, Baiker A, Wokaun A (1996) Langmuir 12: 5319–5329
20. Collins SE, Baltanás MA, Bonivardi AL (2004) J Catal 226:410–421
21. Collins SE, Chiavassa DL, Bonivardi AL, Baltanás MA (2005) Catal Lett 103:83–88
22. Collins SE, Delgado JJ, Mira C, Calvino JJ, Bernal S, Chiavassa DL, Baltanás MA, Bonivardi AL (2012) J Catal 292:90–98

23. Pan Y-x, Kuai P, Liu Y, Ge Q, Liu C-j (2010) Energy Environ Sci 3: 1322–1325
24. Zhao B, Pan Y-x, Liu C-j (2012) Catal Today 194:60–64
25. Chiavassa DL, Collins SE, Bonivardi AL, Baltanás MA (2009) Chem Eng J 150:204–212
26. Reimers WG, Baltanás MA, Branda MM (2013) Appl Surf Sci 274:1–6
27. Pan Y-x, Liu C-j, Mei D, Ge Q (2010) Langmuir 26:5551–5558
28. Yang Y, Zhang P (2010) Phys Lett A 374:4169–4173
29. Pan Y-x, Mei D, Liu C-j, Ge Q (2011) J Phys Chem C 115:10140–10146
30. Kohl D, Ochs T, Geyer W, Fleischer M, Meixner H (1999) Sensors Actuators B Chem 59:140–145
31. Gonzalez EA, Jasen PV, Juan A, Collins SE, Baltanás MA, Bonivardi AL (2005) Surf Sci 575:171–180
32. Calatayud M, Collins SE, Baltanas MA, Bonivardi AL (2009) PCCP 11:1397–1405
33. Branda MM, Collins SE, Castellani NJ, Baltanás MA, Bonivardi AL (2006) J Phys Chem B 110:11847–11853
34. Bermudez VM (2008) Langmuir 24:12943–12952
35. Tsai M-Y, Bierwagen O, White ME, Speck JS (2010) J Vac Sci Technol A 28:354–359
36. Oshima T, Arai N, Suzuki N, Ohira S, Fujita S (2008) Thin Solid Films 516:5768–5771
37. Chun HJ, Choi YS, Bae SY, Seo HW, Hong SJ, Park J, Yang H (2003) J Phys Chem B 107:9042–9046
38. Zhan J, Bando Y, Hu J, Xu F, Golberg D (2005) Small 1:883–888
39. Dai L, You LP, Duan XF, Lian WC, Qin GG (2004) J Cryst Growth 267:538–542
40. Hu JQ, Li Q, Zhan JH, Jiao Y, Liu ZW, Ringer SP, Bando Y, Golberg D (2008) ACS Nano 2:107–112
41. Zhu F, Yang ZX, Zhou WM, Zhang YF (2006) Solid State Commun 137:177–181
42. Sharma S, Sunkara MK (2002) J Am Chem Soc 124:12288–12293
43. Chang KW, Wu JJ (2004) Adv Mater 16:545–549
44. Zhang J, Liu ZG, Lin CK, Lin J (2005) J Cryst Growth 280:99–106
45. Sun XM, Li YD (2004) Angew Chem Int Ed 43:3827–3831
46. Zhou X, Qu J, Xu F, Hu J, Foord JS, Zeng Z, Hong X, Edman Tsang SC (2013) Chem Commun 49:1747–1749
47. Kresse G, Hafner J (1993) Phys Rev B 47:558–561
48. Kresse G, Hafner J (1994) Phys Rev B 49:14251–14269
49. Kresse G, Furthmüller J (1996) Comput Mater Sci 6:15–50
50. Kresse G, Furthmüller J (1996) Phys Rev B 54:11169–11186
51. Blöchl PE (1994) Phys Rev B 50:17953–17979
52. Kresse G, Joubert D (1999) Phys Rev B 59:1758–1775
53. Perdew JP, Burke K, Ernzerhof M (1996) Phys Rev Lett 77:3865–3868
54. Perdew JP, Burke K, Ernzerhof M (1997) Phys Rev Lett 78:1396
55. Bader RFW (1990) Atoms in molecules—a quantum theory. Clarendon, Oxford
56. Tang W, Sanville E, Henkelman G (2009) J Phys Condens Matter 21: 084204
57. Sanville E, Kenny SD, Smith R, Henkelman G (2007) J Comput Chem 28:899–908
58. Henkelman G, Arnaldsson A, Jonsson H (2006) Comput Mater Sci 36:354–360
59. Jonsson H, Mills G, Jacobsen KW (1998) Nudged elastic band method for finding minimum energy paths of transitions. World Scientific, Singapore
60. Henkelman G, Jónsson H (2000) J Chem Phys 113:9978–9985
61. Henkelman G, Uberuaga BP, Jónsson H (2000) J Chem Phys 113: 9901–9904
62. Sheppard D, Terrell R, Henkelman G (2008) J Chem Phys 128: 134106
63. Sheppard D, Henkelman G (2011) J Comput Chem 32:1769–1771
64. Sheppard D, Xiao P, Chemelewski W, Johnson DD, Henkelman G (2012) J Chem Phys 136:074103